Article

Bond Selection in the Photoisomerization Reaction of Anionic Green Fluorescent Protein and Kindling Fluorescent Protein Chromophore Models

Seth Olsen, and Sean C. Smith

J. Am. Chem. Soc., **2008**, 130 (27), 8677-8689 • DOI: 10.1021/ja078193e • Publication Date (Web): 14 June 2008

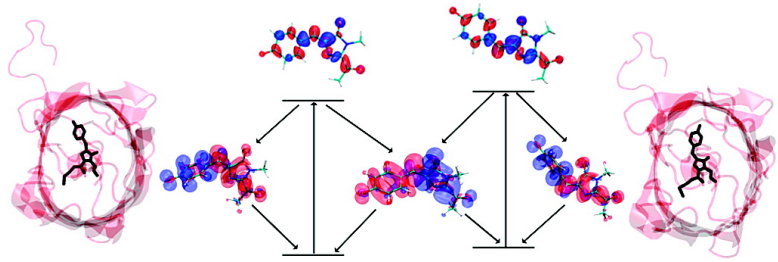

J|A|C|S
ARTICLES

Published on Web 06/14/2008

Bond Selection in the Photoisomerization Reaction of Anionic Green Fluorescent Protein and Kindling Fluorescent Protein Chromophore Models

Seth Olsen*,† and Sean C. Smith

Centre for Computational Molecular Science, Australian Institute for Bioengineering and Nanotechnology, The University of Queensland, St. Lucia, QLD 4072 Australia

Received October 25, 2007; E-mail: s.olsen1@uq.edu.au

Abstract: The chromophores of the most widely known fluorescent proteins (FPs) are derivatives of a core *p*-hydroxybenzylidene-imidazolinon-5-one (HBI) motif, which usually occurs as a phenolate anion. Double bond photoisomerization of the exocyclic bridge of HBI is widely held to be an important internal conversion mechanism for FP chromophores. Herein we describe the ground and excited-state electronic structures and potential energy surfaces of two model chromophores: 4-*p*-hydroxybenzylidiene-1,2-dimethyl-imidazolin-5-one anion (HBDI), representing green FPs (GFPs), and 2-acetyl-4-hydroxybenylidene-1-methyl-imidazolin-5-one anion (AHBMI), representing kindling FPs (KFPs). These chromophores differ by a single substitution, but we observe qualitative differences in the potential energy surfaces which indicate inversion of bond selection in the photoisomerization reaction. Bond selection is also modulated by whether the reaction proceeds from a *Z* or an *E* conformation. These configurations correspond to fluorescent and nonfluorescent states of structurally characterized FPs, including some which can be reversibly switched by specific illumination regimes. We explain the difference in bond selectivity via substituent stabilization effects on a common set of charge-localized chemical structures. Different combinations of these structures give rise to both optically active (planar) and twisted intramolecular charge-transfer (TICT) states of the molecules. We offer a prediction of the gas-phase absorption of AHBMI, which has not yet been measured. We offer a hypothesis to explain the unusual fluorescence of AHBMI in DMF solution, as well as an experimental proposal to test our hypothesis.

Introduction

The fluorescent proteins (FPs) are homologues of the green fluorescent protein (GFP)[1] from the jellyfish *Aequorea victoria*. They have spawned a profusion of useful biotechnologies.[2] The catalogue of naturally occurring FPs has expanded dramatically since the beginning of the century.[3] Subfamilies are categorized by variations in their chromophores, many of which are derivatives of a common *p*-hydroxybenzylidene-imidazolin-5-one (HBI) motif[4] in a (phenolate) anionic form. The HBI anion motif is displayed in Figure 1, in two distinct bridge conformations. Dual bonding structures can be drawn, as indicated in Figure 1, creating a resonant π orbital system with a strongly absorbing S_1 excited state.

FPs are useful because of their fluorescence properties. There is therefore much interest in competing nonradiative decay mechanisms. Mounting evidence suggests photoisomerization of the bridge of the chromophore is a major, perhaps predominant, mechanism of radiationless decay in FP chromophores in solution[5–11] and in proteins[12–15] following excitation into the

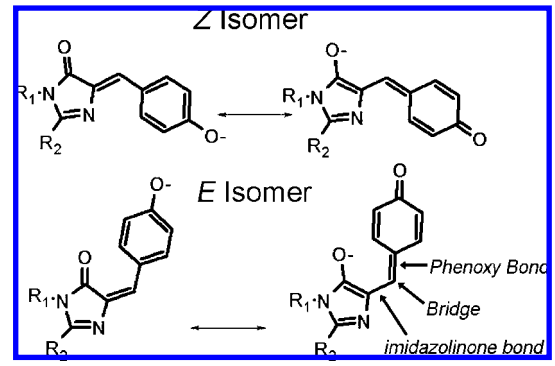

Figure 1. The HBI motif in an anionic protonation state. Resonant structures can be drawn for the anion which differ by bridge bond alternation and by localization of the excess charge. Isomerization of the imidazolinone bond switches between distinct *Z* and *E* isomeric forms. Isomerization of the phenoxy bond leaves the structure unchanged. *Z* and *E* isomeric forms are often referred to as cis or trans, respectively.

† Current address: Centre for Organic Photovoltaics & Electronics, School of Physical Sciences, The University of Queensland, St. Lucia, QLD 4072 Australia.

(1) Tsien, R. Y. *Annu. Rev. Biochem.* **1998**, *67*, 509–544.
(2) Verkusha, V. V.; Lukyanov, K. A. *Nat. Biotechnol.* **2004**, *22* (3), 289–296.
(3) Shagin, D. A.; Barsova, E. V.; Yanushevich, Y. G.; Fradkov, A. F.; Lukyanov, K. A.; Labas, Y. A.; Semenova, T. N.; Ugalde, J. A.; Meyers, A.; Nunez, J. M.; Widder, E. A.; Lukyanov, S. A.; Matz, M. V. *Mol. Biol. Evol.* **2004**, *21* (5), 841–849.
(4) Remington, S. J. *Curr. Opin. Struct. Biol.* **2006**, *16* (6), 714–721.
(5) Gepshtein, R.; Huppert, D.; Agmon, N. *J. Phys. Chem.* **2006**, *B110* (9), 4434–4442.
(6) Litvinenko, K. L.; Webber, N. M.; Meech, S. R. *J. Phys. Chem.* **2003**, *A107*, 2616–2623.
(7) Mandal, D.; Tahara, T.; Meech, S. *J. Phys. Chem.* **2004**, *B108* (3), 1102–1108.

bright lowest-lying singlet $\pi\pi^*$ state[16] of the chromophore. Excitation from the resonant ground-state generates the (anti-resonant) twin excited state,[17] which favors twisting about one or both of the bridge bonds, leading to twisted S_1 intermediates[18–21] and nearby low-lying conical intersection seams.[20–23] Previous studies of GFP and red fluorescent protein (RFP) chromophores determined that the internal conversion is mediated by conical intersections between twisted intramolecular charge-transfer (TICT) states of opposing polarity.[19–24] The ordering of the TICT states, their stabilities relative to the Franck−Condon region, the existence of intermediates in the TICT manifold, and the accessibility of the relevant intersections are influenced by solvent[18] and substituent[21] effects. These facets of the TICT manifold help explain the fluorescence quantum yield dependence for a series of synthetic HBI derivatives[25] in solvents with different dielectric constants.

Some FPs can be reversibly switched between bulk fluorescent and nonfluorescent states by specific illumination regimes.[26] These show promise in novel imaging techniques[27] and as bases for all-optical memory.[28] Crystallographic studies[29–32] indicate that bright and dark states are distinguished by *Z*/*E* isomerism of the bond connecting the imidazolinone to the methine bridge (herein referred to as the 'imidazolinone bond'). This behavior is best known within the 'kindling' (KFP) subfamily[33] to which the asFP595 protein[34] belongs. Figure 2 displays an suitable example, the A143S mutant of asFP595, in its native (nonfluorescent) and switched (fluorescent) states and shows the change in chromophore configuration between them.[31] *Z*/*E* isomerism of the imidazolinone bond also distinguishes bright and dark states in non-photoswitchable proteins.[35–38] The thermal isomerization of a GFP chromophore anion in aqueous solution has been experimentally characterized.[39] The *Z* isomer was determined to be more stable by 2.3 kcal/mol, and the activation barrier for the (ground state) isomerization was determined to be 13.1 kcal/mol. The reader should note that the *Z* isomer is often called cis in the fluorescent protein literature and the *E*

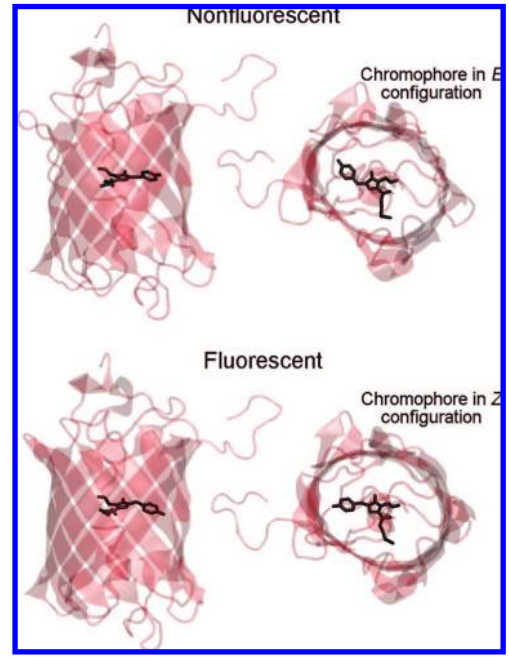

Figure 2. Nonfluorescent (top) and fluorescent (bottom) states of the A143S mutant of asFP595 protein, a member of the KFP subfamily. In the nonfluorescent dark-adapted state, the chromophore is in a nonplanar *E* configuration. High-intensity illumination near the absorbance maximum switches the protein to a fluorescent state with a planar *Z* chromophore. Back-switching can be accomplished by higher energy light at moderate intensities. Images were rendered from structures reported in ref 31.

(8) Mandal, D.; Tahara, T.; Webber, N. M.; Meech, S. R. *Chem. Phys. Lett.* **2002**, *358* (5−6), 495–501.
(9) Usman, A.; Mohammed, O. F.; Nibbering, E. T. J.; Dong, J.; Solntsev, K. M.; Tolbert, L. M. *J. Am. Chem. Soc.* **2005**, *127* (32), 11214–11215.
(10) Vengris, M.; Stokkum, I. H. M. v.; He, X.; Bell, A. F.; Tonge, P. J.; Grondelle, R. v.; Larsen, D. S. *J. Phys. Chem.* **2004**, *A108*, 4587–4598.
(11) Webber, N. M.; Konstantin, L.; Litvinenko, L.; Meech, S. R. *J. Phys. Chem.* **2001**, *B105*, 8036–8039.
(12) Kummer, A.; Kompa, C.; Lossau, H.; Pöllinger-Dammer, F.; Michel-Beyerle, M.; Silva, C. M.; Bylina, E. J.; Coleman, W. J.; Yang, M. M.; Youvan, D. C. *Chem. Phys.* **1998**, *237*, 183–193.
(13) Litvinenko, K. L.; Meech, S. R. *Phys. Chem. Chem. Phys.* **2004**, *6* (9), 2012–2014.
(14) Stavrov, S. S.; Solntsev, K. M.; Tolbert, L. M.; Huppert, D. *J. Am. Chem. Soc.* **2006**, *128* (5), 1540–1546.
(15) Winkler, K.; Lindner, J.; Subramaniam, V.; Jovin, T. M.; Vöhringer, P. *Phys. Chem. Chem. Phys.* **2002**, *4* (6), 1072–1081.
(16) Helms, V.; Winstead, C.; Langhoff, P. W. *J. Mol. Struct. (THEOCHEM)* **2000**, *506*, 179–189.
(17) Zilberg, S.; Haas, Y. *J. Phys. Chem.* **1998**, *A102* (52), 10843–10850.
(18) Altoe, P.; Bernardi, F.; Garavelli, M.; Orlandi, G.; Negri, F. *J. Am. Chem. Soc.* **2005**, *127* (11), 3952–3963.
(19) Martin, M. E.; Negri, F.; Olivucci, M. *J. Am. Chem. Soc.* **2004**, *126*, 5452–5464.
(20) Olsen, S. Ph.D. Thesis, The University of Illinois at Urbana-Champaign, Urbana, IL, 2004.
(21) Olsen, S.; Smith, S. C. *J. Am. Chem. Soc.* **2007**, *129* (7), 2054–2065.
(22) Toniolo, A.; Granucci, G.; Martinez, T. J. *J. Phys. Chem.* **2003**, *A107*, 3822–3830.
(23) Toniolo, A.; Olsen, S.; Manohar, L.; Martinez, T. J. *Faraday Discuss.* **2004**, *129*, 149–163.
(24) Toniolo, A.; Olsen, S.; Manohar, L.; Martínez, T. J. Ultrafast Excited State Dynamics in Green Fluorescent Protein Chromophore. In *Femtochemistry and Femtobiology: Ultrafast Events in Molecular Science*; Martin, M., Hynes, J. T., Eds.; Elsevier: Amsterdam, 2004.
(25) Follenius-Wund, A.; Bourotte, M.; Schmitt, M.; Iyice, F.; Lami, H.; Bourguignon, J.-J.; Haiech, J.; Pigault, C. *Biophys. J.* **2003**, *85*, 1839–1850.
(26) Henderson, J. N.; Remington, S. J. *Physiology* **2006**, *21*, 162–170.
(27) Hofmann, M.; Eggeling, C.; Jakobs, S.; Hell, S. W. *Proc. Natl. Acad. Sci. U.S.A.* **2005**, *102*, 17565–17569.
(28) Chirico, G.; Cannone, F.; Diaspro, A.; Bologna, S.; Pellegrini, V.; Nifosì, R.; Beltram, F. *Phys. Rev.* **2004**, *E70*, 030901.
(29) Henderson, J. N.; Ai, H.-w.; Campbell, R. E.; Remington, S. J. *Proc. Natl. Acad. Sci. U.S.A.* **2007**, *104* (16), 6672–6677.
(30) Quillin, M. L.; Anstrom, D. M.; Shu, X.; O'Leary, S.; Kallio, K.; Chudakov, D. M.; Remington, S. J. *Biochem.* **2005**, *44* (15), 5774–5787.
(31) Andresen, M.; Wahl, M. C.; Stiel, A. C.; Grater, F.; Schafer, L. V.; Trowitzsch, S.; Weber, G.; Eggeling, C.; Grubmuller, H.; Hell, S. W.; Jakobs, S. *Proc. Natl. Acad. Sci. U.S.A.* **2005**, *102* (37), 13070–13074.
(32) Wilmann, P. G.; Petersen, J.; Devenish, R. J.; Prescott, M.; Rossjohn, J. *J. Biol. Chem.* **2005**, *280* (4), 2401–2404.
(33) Chudakov, D. M.; Feofanov, A. V.; Mudrick, N. N.; Lukyanov, S.; Lukyanov, K. A. *J. Biol. Chem.* **2003**, *278* (9), 7215–7219.
(34) Lukyanov, K. A.; Fradkov, A. F.; Gurskaya, N. G.; Matz, M. V.; Labas, Y. A.; Savitsky, A. P.; Markelov, M. L.; Zaraisky, A. G.; Zhao, X.; Fang, Y.; Tan, W.; Lukyanov, S. A. *J. Biol. Chem.* **2000**, *275* (34), 25879–25882.
(35) Henderson, J. N.; Remington, S. J. *Proc. Natl. Acad. Sci. U.S.A.* **2005**, *102* (36), 12712–12717.
(36) Tretyakova, Y. A.; Pakhomov, A. A.; Martynov, V. I. *J. Am. Chem. Soc.* **2007**, *129* (25), 7748–7749.
(37) Wilmann, P. G.; Battad, J.; Beddoe, T.; Olsen, S.; Smith, S. C.; Dove, S.; Devenish, R. J.; Rossjohn, J.; Prescott, M. *Photochem. Photobiol.* **2006**, *82* (2), 359–366.
(38) Wilmann, P. G.; Petersen, J.; Pettikiriarachchi, A.; Buckle, A. M.; Smith, S. C.; Olsen, S.; Perugini, M. A.; Devenish, R. J.; Prescott, M.; Rossjohn, J. *J. Mol. Biol.* **2005**, *349*, 223–237.
(39) He, X.; Bell, A.; Tonge, P. J. *FEBS Lett.* **2003**, *549*, 35–38.

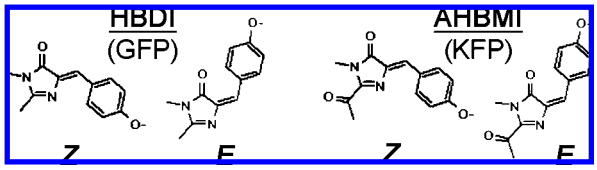

Figure 3. Chemical structures of HBDI (left) and AHBMI (right), the chromophore models studied in this work. HBDI is a model of the chromophore of the GFP subfamily. AHBMI is a model of the chromophore of the KFP subfamily.

isomer called trans. In this work we will use *Z* and *E* in accord with organic chemical naming conventions.[40]

Only the imidazolinone bond can function as a *Z*/*E*-isomeric switch between distinct populations of an anionic FP chromophore. The phenoxy bond cannot because the para configuration of the phenoxy means isomerization maps the starting conformation to itself. However, photoisomerization of either bond has been linked to internal conversion via conical intersection seams.[18–24] This suggests that selection between photoswitching and ground-state recovery in protein corresponds, at atomic resolution, to selection between different photoisomerization outcomes for the chromophore.

In this paper, we will present multistate quantum chemical results for chromophores of the GFP and KFP subfamilies. These contain members for which *Z*/*E* photoswitching has been implicated by direct structural evidence.[29–32] We examine GFP and KFP chromophore models side by side using size extensive correlated electronic structure methods. We will focus particular attention on differences in the excited-state surfaces which may influence bond selection in the photoisomerization reaction, as indicated by the presence and energetic ordering of TICT intermediates, the accessibility of nearby intersections and the excited-state energies along chemically motivated photoisomerization coordinates. The selection patterns which we observe seem to be readily understandable in terms of the ground-state resonance (Figure 1) and excited-state antiresonance between charge-localized electronic structures for the chromophore.

Computational Methodology. We will present results for two model chromophores. The first, *p*-hydroxybenzylidiene-1,2-dimethyl-imidazolin-5-one anion (HBDI) represents the GFP subfamily. The second, 2-acetyl-4-hydroxybenylidene-1-methyl-imidazolin-5-one anion (AHBMI) represents the KFP subfamily. The structures of these chromophores are shown in Figure 3 in their *Z* and *E* configurations. Both are all-atom representations of synthetic model chromophores for which various experimental results have been reported.[41,42] The reader should note that the *Z* isomer is often referred to as cis in the fluorescent protein literature, and the *E* isomer as trans.

Our electronic wave functions were generated via dynamically correlated multistate electronic structure computations built upon a state-averaged[43] complete active space self-consistent field[44] (SA-CASSCF) reference wave function, using geometries optimized at the SA-CASSCF level. We have chosen an active space according to a specific chemical abstraction, outlined in Figure 4, which is focused on the bridge bonding chemistry. This active space is spanned by three (Boys) localized[45] orbitals centered on the phenoxy, bridge, and imidazolinone moieties. It is the simplest wave function which can describe a bond and an excess electron resonating between three π orbitals on distinct sites. The many-electron space can be spanned by a basis of three valence-bond structures, each of which carries contributions from three *formally covalent* structures, which we label as Φ_P^-, Φ_B^-, and Φ_I^- (according to the identity of the doubly filled orbital) and three *formally ionic* structures Φ_P^+, Φ_B^+, and Φ_I^+ (according to the identity of the empty orbital, see Figure 4). We have found that the structure of this variational model space is stable across all geometries investigated, in the sense that the structure of the Boys orbitals changes very little with respect to the frame of the associated fragment, and these small changes are continuous with respect to geometric changes. We optimized the orbitals in our CASSCF to minimize an evenly weighted average of the three lowest-lying singlet states of the reference space. This corresponds to one perfect pairing degree of freedom for each state in the average. The three-state average should help avoid spurious barriers which may arise when the character of an adiabatic state changes (as in the $Li^+ + H_2$ reaction[43]). We have previously observed[20] a pseudo-Jahn−Teller

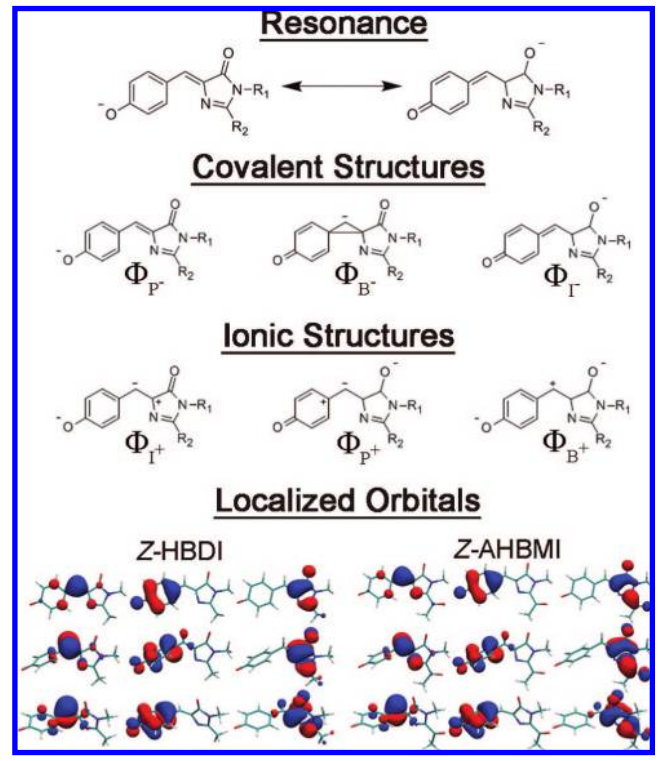

Figure 4. Graphical representation of our bridge-focused SA-CASSCF active space. Top: Canonical resonance for anionic HBI derivatives. Middle: Covalent (upper middle) and ionic (lower middle) valence bond structures used to interpret the electronic structure. Bottom: Localized orbitals on the bridge (ϕ_B), phenoxy (ϕ_P), and imidazolinone (ϕ_I) which span the SA3-CAS(4,3) active space of *Z*-HBDI (left) and *Z*-AHBMI (right). Similar orbitals are used for the *E* isomers. Analogous orbitals are organized within columns. Rows correspond to planar (top), phenoxy-twisted (middle), and imidazolinone-twisted (bottom) geometries. The shape of the orbital on each fragment stays the same.

(40) Solomons, T. G. W. *Organic Chemistry*, 6th ed.; John Wiley & Sons: New York, 1996; p 1328.
(41) Yampolsky, I. V.; Remington, S. J.; Martynov, V. I.; Potapov, V. K.; Lukyanov, S.; Lukyanov, K. A. *Biochemistry* **2005**, *44*, 5788–5793.
(42) Kojima, S.; Hirano, T.; Niwa, H.; Ohashi, M.; Inouye, S.; Tsuji, F. I. *Tetrahedron Lett.* **1997**, *38* (16), 2875–2878.
(43) Docken, K. K.; Hinze, J. *J. Chem. Phys.* **1972**, *57* (11), 4928–4936.
(44) Roos, B. O. The Complete Active Space Self-Consistent Field Method and Its Applications in Electronic Structure Calculations. In *Ab Initio Methods in Quantum Chemistry II*; Lawley, K. P., Ed.; John Wiley and Sons: New York, 1987; p 399.
(45) Foster, J. M.; Boys, S. F. *Rev. Mod. Phys.* **1960**, *32* (2), 300.

effect[46] in the S_1 surface of a planar GFP chromophore anion which arises from degeneracy of one-electron states on the phenoxy and imidazolinone. Averaging over the S_2 state also avoids artifacts which may result from the associated S_1/S_2 coupling. We will refer to our CASSCF model as SA3-CAS(4,3). This reference wave function was used without dynamical correlation to generate optimized molecular structures on the S_0 and S_1 states, as well as S_1/S_0 minimal energy conical intersections (MECIs).[47] To evaluate energies at these geometries, we corrected the SA3-CAS(4,3) energies with dynamical correlation contributions via multireference, multistate second-order Rayleigh−Schrödinger perturbation theory (MR-MS-RSPT2).[48] In this perturbation theory, the reference space is remixed as the perturbation is applied, and the states are obtained by diagonalization of a symmetrized perturbed effective Hamiltonian. The remixing of the reference space was modest at all geometries. Due to limitations associated with 64-bit integers, only 32 orbitals could be correlated in the MS-RSPT2 calculations. This should be sufficient to describe correlations within the π system, as well as some low-energy correlations within the σ system and between the σ and π systems. A level shift of 0.1 h was applied to all of the RSPT2 calculations[49] to facilitate convergence of the perturbation expansion. MR-MS-RSPT2 provides size-consistent energies. Some deviation from size-consistency may arise from truncation of the correlated orbital set. We used a Dunning double-ζ basis set with polarization functions on all atoms (DZP)[50,51] as our one-electron basis. We also calculated certain electronic properties, such as dipole moments, oscillator strengths, and electron densities, at the SA3-CAS(4,3)/DZP optimized structures. These properties were computed using internally contracted multireference configuration interaction with single and double substitutions (MR-CISD).[52] Limits on the correlated orbital set were the same as for the MR-MS-RSPT2. Rayleigh−Schrödinger perturbation theory does not give size-consistent densities and exhibits other problems (density traces not yielding proper electron numbers, etc.) which are avoided by MRCISD. All of the results were obtained with the Molpro[53] program.

We are interested in bridge torsion. As quantitative measures of bond twisting we will make use of torsion coordinates τ_I and τ_P, which we will define as averages of primitive dihedrals taken on either side of the bonds. As an illustrative example, such a torsion coordinate for 1,3-deutero-ethylene would be equal to the average of dihedrals defined by 1D-C=C-3D and 4H−C=C-2H (with that ordering). The coordinates are visually summarized in Figure 5. Defining the torsion in this way helps to avoid problems associated with dependency between the dihedrals and hybridization/pyramidalization parameters at the atomic sites. We will use the $\theta_{\sigma\pi}$ angle defined by Haddon[54] as a measure of pyramidalization of an atomic site. This is the angle subtended by the π orbital axis vector and the σ bond framework of the pyramidalized atom. Its value is 90° for a planar carbon, 101° for any site in a buckminsterfullerene molecule, and 109° for a tetrahedral carbon atom.

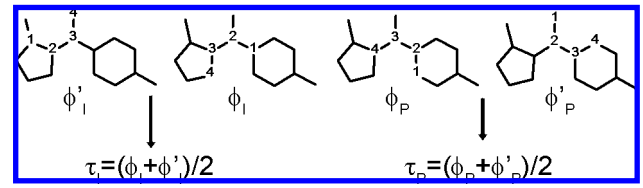

Figure 5. Definition of the bridge torsion coordinates τ_I and τ_P in terms of a set of four primitive dihedral angles spanning the bridge. Torsion coordinates are defined as equally weighted averages of two dihedrals defined over a given bond. Dihedral angles are defined as the angle between planes spanned by atoms 1, 2, 3 and 2, 3, 4 in the indicated numbering scheme.

In order to obtain a broader view of the photoisomerization, we calculated energies and properties along coordinate-driven slices through the potential energy surfaces. These were obtained via optimization on the S_1 state subject to constraints on the τ_I and τ_P torsion coordinates. For each point, one torsion coordinate was constrained to a constant while the other was constrained to zero and the remaining degrees of freedom were optimized on the SA3-CAS(4,3) S_1 surface. Quantitative activation energies cannot be obtained from such slices, although they provide an upper bound to the activation energy in the limit of sufficient sampling.

Results

S_0 and S_1 Energetics. We optimized *Z* and *E* minima (called *Z*-Min-S_0 and *E*-Min-S_0) of HBDI and AHBMI on the S_0 state, as well as S_1 intermediates (minima) which are twisted at the phenoxy bond (*Z,E*-P-S_1) or at the imidazolinone bond (I-S_1). We also optimized planar structures on the S_1 surface (*Z,E*-Plan-S_1), under the constraint of a planar bridge ($\tau_I = \tau_P = 0$). Finally, we obtained S_0/S_1 minimal energy conical intersection (MECI) geometries which are twisted about the phenol-bridge (*Z,E*-P-$S_{0/1}$) and imidazolinone-bridge bond (I-$S_{0/1}$). The S_0 and S_1 energies of these structures evaluated with SA3-CAS(4,3) and with MR-MS-RSPT2 are illustrated in Figure 6 (HBDI) and in Figure 7 (AHBMI). S_0-S_1 electron density difference isosurfaces calculated at the MRCISD level at the *Z,E*-Min-S_0, *Z,E*-P-S_1 and I-S_1 geometries are also displayed. The isosurfaces evaluated at the *Z,E*-Plan-S_1 geometries were qualitatively identical to those generated at the *Z,E*-S_0 geometries. Previous vibrational analyses of HBDI[18] and HBI[19] have confirmed that the twisted intermediates are true stable minima on the potential surface. Preliminary tests verified this also for AHBMI.

The S_0 and S_1 energies at the *E*-Min-S_0 structures are higher than at the corresponding *Z* structures. There is a much smaller difference between *Z* and *E* conformers at the P-S_1 structures or the P-$S_{0/1}$ intersections than at the Min-S_0 structures. The net effect is that the *E* planar structures are more destabilized relative to the phenoxy-twisted geometries relative to the *Z* isomers and have a greater number of twisted intermediates and MECIs which are energetically available to them. This is true for both HBDI and AHBMI. The energetic ordering of the I-S_1 and *Z,E*-P-S_1 intermediates (and the associated MECIs) are reversed between HBDI and AHBMI. In HBDI, the I-S_1 structure lies 11 kcal/mol below *Z*-Min-S_0 and 14 kcal/mol below *E*-Min-S_0 on the S_1 surface; it also lies 7 kcal/mol below *Z*-Plan-S_1 and 10 kcal/mol below *E*-Plan-S_1. In AHBMI, the

(46) Jahn, H. A.; Teller, E. *Proc. R. Soc. London* **1937**, *A161* (905), 220–235.
(47) Levine, B. G.; Martinez, T. J. *Annu. Rev. Phys. Chem.* **2007**, *58* (1), 613–634.
(48) Finley, J.; Malmqvist, P.-A.; Roos, B. O.; Serrano-Andres, L. *Chem. Phys. Lett.* **1998**, *288* (2−4), 299–306.
(49) Roos, B. O.; Andersson, K. *Chem. Phys. Lett.* **1995**, *245* (2−3), 215–223.
(50) Dunning, T. H. *J. Chem. Phys.* **1970**, *53*, 2823.
(51) Dunning, T. H.; Hay, P. J. In *Methods of Electronic Structure*; Shaefer, H. F., III, Ed.; Plenum Press: New York, 1977; Vol. 2.
(52) Werner, H.-J.; Knowles, P. J. *J. Chem. Phys.* **1988**, *89* (9), 5803–5814.
(53) Werner, H.-J. MOLPRO, a package of ab initio programs, version 2006.1.
(54) Haddon, R. C. *J. Am. Chem. Soc.* **1990**, *112* (9), 3385–3389.

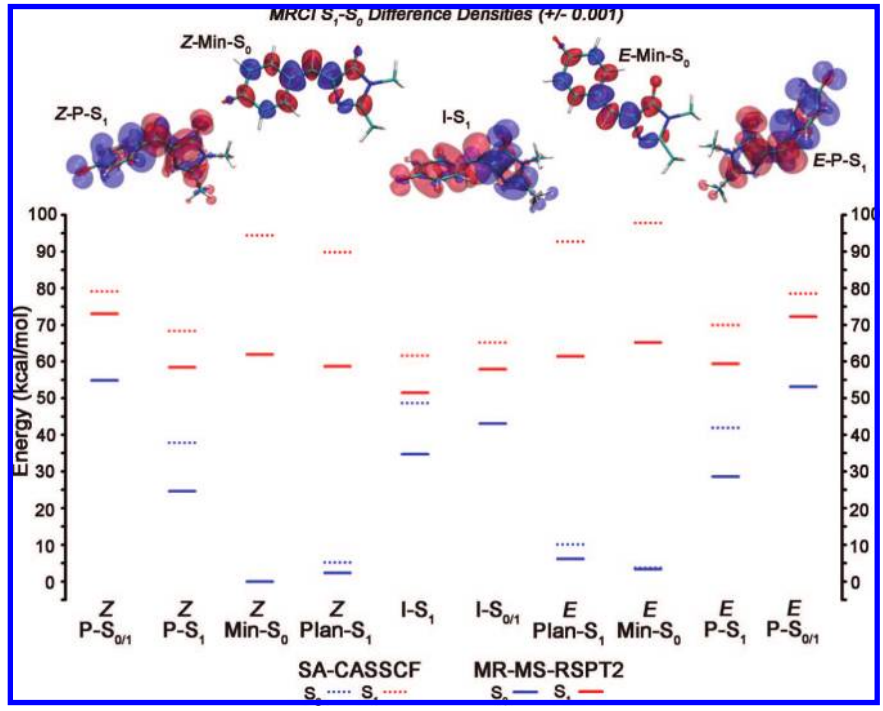

Figure 6. Energy diagram for the S_0 and S_1 states of HBDI anion at the SA3-CAS(4,3)/DZP potential surface extrema, calculated at SA-CASSCF and MR-MS-RSPT2 levels. MRCISD S_1-S_0 difference densities (isovalue = +/−0.001) for the *Z*,*E*-Min-S_0, *Z*,*E*-P-S_1 and I-S_1 geometries are displayed at the top. Blue isosurfaces indicate density depletion; red isosurfaces indicate gain.

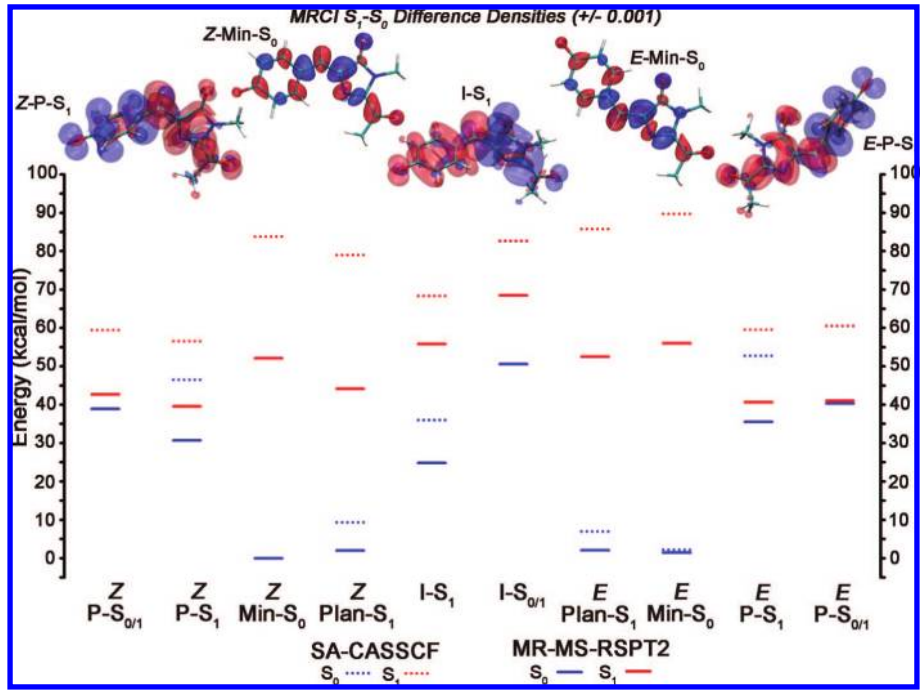

Figure 7. Energy diagram for the S_0 and S_1 states of AHBMI anion at the SA3-CAS(4,3)/DZP potential surface extrema, calculated at SA-CASSCF and MR-MS-RSPT2 levels. MRCISD S_1-S_0 difference densities (isovalue = +/−0.001) for the *Z*,*E*-Min-S_0, *Z*,*E*-P-S_1 and I-S_1 geometries are displayed at the top of the figure. Blue isosurfaces indicate density depletion; red isosurfaces indicate gain.

I-S_1 structure is 1 kcal/mol above the *Z*-Min-S_0 S_1 energy and 2 kcal/mol below *E*-Min-S_0. It is isoenergetic on S_1 with the *E*-Plan-S_1 structure. These trends are reversed for the P-S_1 intermediates. In HBDI, the S_1 energy of the *Z*-P-S_1 structure lies 4 kcal/mol beneath *Z*-Min-S_0 and is isoenergetic with *Z*-Plan-S_1, while *E*-P-S_1 is 6 kcal/mol beneath *E*-Min-S_0 and 2 kcal/mol beneath *E*-Plan-S_1. In AHBMI, *Z*-P-S_1 is 11 kcal/mol beneath *Z*-Min-S_0 and 2 kcal/mol beneath *Z*-Plan-S_1, while *E*-P-S_1 is 14 kcal/mol beneath *E*-Min-S_0 and 12 kcal/mol beneath *E*-Plan-S_1. The S_1 energy of the P-$S_{0/1}$ intersections of HBDI is inaccessible from *Z* and *E*-Min-S_0. The MECIs on the SA3-CAS(4,3) surfaces are also not strictly intersections on the MR-MS-RSPT2 surfaces because correlation splits the degeneracy by 18−19kcal/mol. The degeneracy at the I-$S_{0/1}$ MECI in HBDI is also split, by 15 kcal/mol. If we approximate the energies of the MECIs on the MR-MS-RSPT2 surfaces by an *average* of

Table 1. MR-MS-RSPT2 Calculated S0-S1 Excitation Energies (eV), MRCISD Oscillator Strengths, S_0 and S_1 Dipole Moment norms (D) and Angle Subtended by S_0 and S_1 Dipole Vectors for Nonintersection SA3-CAS(4,3)/DZP Geometries of HBDI (top) and AHBMI (bottom)

geometry	ΔE (eV)	f	$\|\mu\|(S_0)$ (D)	$\|\mu\|(S_1)$ (D)	$\theta(S_0,S_1)$, deg
			HBDI[a]		
Z-Min-S_0	2.69	1.50	16.7	15.7	1
Z-Plan-S_1	2.44	1.35	16.9	15.6	1
E-Min-S_0	2.68	1.36	18.4	18.3	2
E-Plan-S_1	2.40	1.19	18.1	18.7	1
Z-P-S_1	1.41	0.00	22.8	7.3	9
E-P-S_1	1.31	0.00	25.3	11.0	10
I-S_1	0.66	0.00	9.1	22.5	22
AHBMI[b]					
Z-Min-S_0	2.32	1.44	9.8	10.5	9
Z-Plan-S_1	1.78	1.18	11.5	10.7	10
E-Min-S_0	2.41	1.62	11.8	12.1	4
E-Plan-S_1	2.20	1.48	11.5	12.4	6
Z-P-S_1	0.57	0.00	18.8	4.5	59
E-P-S_1	0.46	0.00	22.0	5.9	45
I-S_1	1.15	0.00	6.7	18.8	57

[a] Gas phase ΔE^{abs}_{max} 2.59 eV.[55] [b] 2-Propanol solution ΔE^{abs}_{max} 2.25 eV.[41]

their S_0 and S_1 energies at the SA3-CAS(4,3) MECIs, we find that the *Z*-P-$S_{0/1}$ intersection is 2 kcal/mol above *Z*-Min-S_0 while *E*-P-$S_{0/1}$ is 1 kcal/mol below *E*-Min-S_0 and 3 kcal/mol above *E*-Plan-S_1. In AHBMI, the averaged energy of the I-$S_{0/1}$ intersection is isoenergetic with *Z*-Min-S_0 and 2 kcal/mol below *E*-Min-S_0. Correlation splits the degeneracy of the AHBMI MECIs by 5, 6, and 3 kcal/mol at the *Z*-P-$S_{0/1}$, *E*-P-$S_{0/1}$, and I-$S_{0/1}$ MECIs, respectively. The averaged energies at the AHBMI MECIs are less than 2 kcal/mol above their corresponding (by identification of the most twisted bond) twisted S_1 intermediates, and the *E*-P-$S_{0/1}$ average energy is actually *lower* than the S_1 energy at *E*-P-S_1. In HBDI, the difference between the average MECI energies and the corresponding intermediates are larger for the P-$S_{0/1}$ intersections while the I-$S_{0/1}$ average energy is lower than the S_1 energy at I-S_1. If the average energy of an MECI is lower than the S_1 energy of the corresponding intermediate, this indirectly suggests that the energy of the intersection optimized at the MS-MR-RSPT2 level may be isoenergetic with the intermediate or supplant it as the minimum on the S_1 surface. This should be verified later for these systems by direct optimization of the MECI on the MR-MS-RSPT2 surfaces.

A good gauge of the accuracy of our approach for electronic structure and geometry is by comparison with the gas-phase absorption maximum of HBDI (2.59 eV)[55] and the absorption maximum for AHBMI in a low dielectric solution (2.25 eV in 2-propanol).[41] We have tabulated excitation energy estimates for all geometries in Table 1, along with MRCISD oscillator strengths, state dipole norms, and angles subtended by the S_0 and S_1 dipoles. The excitations calculated via MR-MS-RSPT2 at the *Z*-Min-S_0 geometries are within 0.1 eV of the experimental absorption maxima and blue-shifted relative to these. If we compare with previously reported theoretical estimates[18] for HBDI, obtained with a larger active space but with less robust single-reference, single-state RSPT2 corrections, we find that our results are also within reasonable agreement and shifted to higher energies. We are not quite in such good accord with a previously reported RSPT2 estimate[56] of the excitation of *Z* and *E* AHBMI but are closer to the experimental absorption maximum. These predicted a higher excitation energy for the *Z* isomer (called cis in that work) than experimentally observed in 2-propanol solution. The reported value for the *E* isomer (trans) was closer to the experimental value and to our result for the *Z* isomer, but this conformer was also predicted to have a higher S_0 energy, contraindicating identification with the experimental absorption maximum.

Planar Structures. The heavy atom bond lengths of the planar Min-S_0 and Plan-S_1 structures for HBDI and AHBMI anions, displayed in Figure 8, show reversed bridge bond length alternation between the *Z* and *E* Plan-S_1 structures. In the *E* isomers, the imidazolinone bond is longer, while in the *Z* isomers, the phenoxy bond is longer. The bridge bond length alternation at the Min-S_0 structures is generally lower in AHBMI than HBDI, and the changes which occur upon descent to the Plan-S_1 structures are more extreme. *Z*-AHBMI, which displays the least alternation in the Min-S_0 structure, has the most alternation at the Plan-S_1 structure. This is also the only case where a bridge bond (specifically, imidazolinone) contracts with relaxation on S_1. Interestingly, *Z*-AHBMI also displays the greatest energy difference between the Min-S_0 and Plan-S_1 structures. The changes in bridge bond lengths upon descent to Plan-S_1 from the Min-S_0 structure for *Z*-HBDI semiquantitatively match those previously reported by Altoe et al.[18] using SA2-CAS(12,11) and a 6-31G* basis[57] and by Helms et al.[16] using a smaller CAS(2,2) active space. The phenoxy CO bond is longer than the imidazolinone CO bond at the *Z*-Min-S_0 and *Z*-Plan-S_1 geometries, also consistent with previous results. It is interesting to note that the comparatively small bridge bond alternation at *Z*-Min-S_0, and large alternation at *Z*-Plan-S_1, which we find in AHBMI resemble more closely previous reports of *Z*-HBI,[19,20] a nonmethylated GFP chromophore model. We postulate that this is due to competing effects of electron-donating methyl groups and an electron-withdrawing carbonyl moiety in the acetyl, whereas HBDI differs from HBI by the addition of only electron-donating methyl substituents.

Analysis of the electronic structure at planar geometries indicates that excitation to S_1 creates a biradicaloid which is delocalized over the bridge. Relaxation on S_1 under constraint of a planar bridge increases somewhat the localization of the biradicaloid on one bond or the other, with strength and sense depending on substituency and initial conformation. The biradical localizes on the phenoxy bond more strongly at the *Z* conformations than at the *E* conformations, and the strength of localization is generally stronger for AHBMI than for HBDI.

TICT Intermediate and MECI Geometries. Upon optimization without constraint on the SA3-CAS(4,3) S_1 surface, both HBDI and AHBMI converge to geometries which are twisted about either the imidazolinone or phenoxy bridge bond. Similar behavior has been observed previously in HBDI,[18] HBI[19,20,22–24,58] and RFP chromophore models.[21] Figure 9 displays selected geometrical details (heavy-atom bond lengths, and selected torsion and bridge pyramidalization parameters) for the twisted S_1 intermediates and twisted S_0/S_1 MECIs. Their relative energies can be found in Figures 6 and 7. The twisted bridge

(55) Nielsen, S. B.; Lapierre, A.; Andersen, J. U.; Pedersen, U. V.; Tomita, S.; Anderson, L. H. *Phys. Rev. Lett.* **2001**, *87*, 228102/1−4.
(56) Amat, P.; Granucci, G.; Buda, F.; Persico, M.; Tozzini, V. *J. Phys. Chem.* **2006**, *B110*, 9348–9353.
(57) Hehre, W. J.; Ditchfield, R.; Pople, J. A. *J. Chem. Phys.* **1972**, *56* (5), 2257–2261.
(58) Weber, W.; Helms, V.; McCammon, J. A.; Langhoff, P. W. *Proc. Natl. Acad. Sci. U.S.A.* **1999**, *96*, 6177–6182.

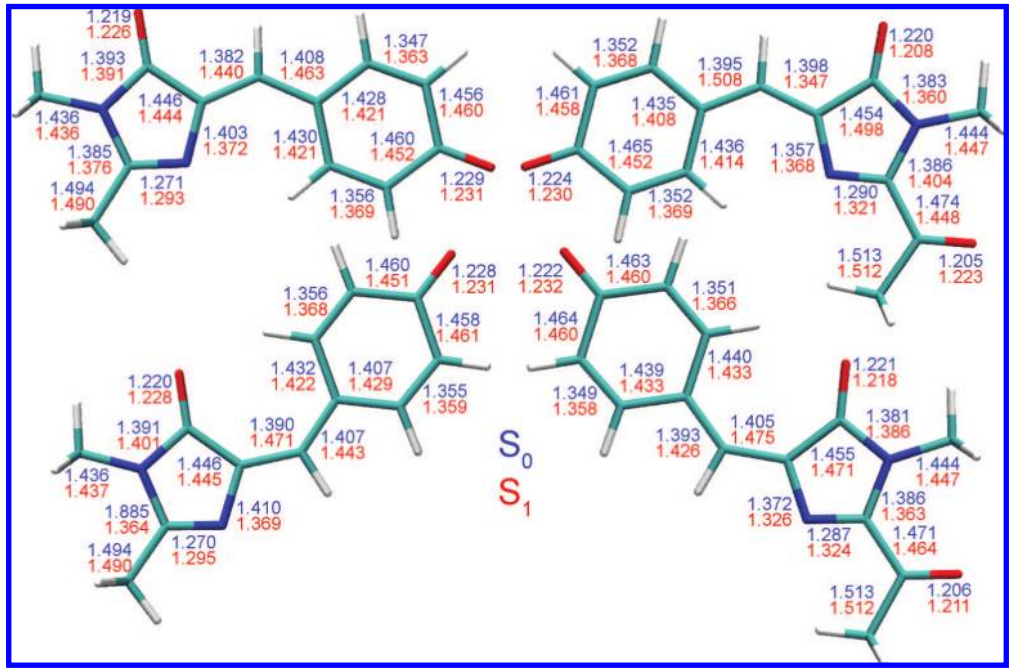

Figure 8. Geometrical details (heavy-atom bond lengths in Å) of the planar extremal structures of *Z*(top) and *E*(bottom) HBDI (left) and AHBMI (right). Blue lettering indicates the Min-S_0 structures; red lettering indicates Plan-S_1. All structures were generated at the SA3-CAS(4,3)/DZP level.

bond is longer than the planar bridge bond in all cases, and the difference between the bridge bond lengths is greater in both HBDI and AHBMI than in previously reported intermediates of HBI calculated with a larger active space.[19,20] The approach from the twisted intermediate geometries to the respective MECIs involves the expansion of both bonds for HBDI, and also in the imidazolinone-twisted case for AHBMI. For phenoxy-twisted *Z* and *E* isomers of AHBMI, the imidazolinone bond contracts while the phenoxy bond expands. The behavior of the CO bonds on the imidazolinone and phenoxy is similar for both HBDI and AHBMI upon moving to the MECI. The CO bond on the twisted fragment contracts and that on the planar fragment expands. The change in the acetyl CO bond in AHBMI between the intermediate and the MECI is insignificant. The changes in the phenoxy bond lengths are consistent with greater aromatic character in the S_1 state if the imidazolinone bond is twisted and greater quinoid character if the phenoxy bond is twisted. The imidazolinone CN bond (positions 2 and 3) expands significantly in AHBMI upon approaching the MECI, whereas the corresponding changes are much smaller in HBDI.

There is no visible pyramidalization of the bridging carbon in AHBMI at the P-$S_{0/1}$ geometries, but such does occur in HBDI at both P-$S_{0/1}$ and I-$S_{0/1}$ MECIs. This indicates that, at the P-S_1 intermediates, a relatively small change in bond polarity (indicated by rehybridization[59]) can induce the degeneracy. The bond length alteration changes required to reach the P-$S_{0/1}$ intersections in AHBMI are also less than for HBDI. On several occasions during the course of data generation we noticed that perturbation theory and configuration interaction were prone to flipping the roots of the reference wave function at the P-$S_{0/1}$ structures of AHBMI. This suggests indirectly that the intersection at correlated levels of theory may be quite close to the P-S_1 twisted intermediate, perhaps even supplanting it as the minimum of the S_1 surface. The I-$S_{0/1}$ geometries of AHBMI display significant bridge pyramidalization, indicating greater perturbation away from the TICT intermediate is required to induce degeneracy. The pyramidalization at the AHBMI *Z*,*E*-P-$S_{0/1}$ geometries, indicated by Haddon's $\theta_{\sigma\pi}$ angle,[54] is closer to the values observed at the P-$S_{0/1}$ geometries of HBDI than the I-$S_{0/1}$ geometries of HBDI. The greater pyramidalization observed at the P-$S_{0/1}$ geometries of HBDI suggests that less perturbation is required to induce degeneracy near the I-S_1 geometry than at the *Z*,*E*-P-S_1 geometries. In short, the overall trend of the geometrical changes separating the twisted intermediates and MECIs suggests opposing tendencies for HBDI and AHBMI. These also parallel the trends in S_0-S_1 energy gaps at the TICT intermediates. Twisted MECIs in HBI also show pyramidalization of the bridge carbon,[19,20] as do imidazolinone-twisted MECIs reported for an RFP chromophore model.[21] In the latter case, the imidazolinone-twisted structures are high in energy while the S_1 minima coincide with phenoxy-twisted MECIs. This behavior of the RFP chromophore model was attributed to the effects of the strongly electron-withdrawing *N*-acylimine substituent on the charge-localized states dominating the TICT manifold.

The S_0-S_1 difference densities (Figures 6 and 7) and state dipole moments (Table 1) at the twisted intermediates are in accord with previous reports[18–21] of FP chromophore anions. Excitation to the S_1 state at these geometries leads to a transfer of charge across the twisted bond from the side opposite to the side adjoining the bridge. Analysis of the electronic structure indicates that the ground-state is dominated by a single covalent Lewis structure with single bond character on the twisted bond and charge localization on the twisted fragment. The S_1 state, on the other hand, features a localized biradicaloid structure over the twisted bond. This is composed of a three-electron π bond between the coplanar fragments, coupled to the twisted ring via a biradical to create an overall singlet.

Coordinate-Driven Potential Energy Surface Slices. Coordinate-driven slices through the S_0 and S_1 potential surfaces of *Z* and

(59) Bonačić-Koutecký, V.; Koutecký, J.; Michl, J. *Angew. Chem., Int. Ed.* **1987**, *26*, 170–189.

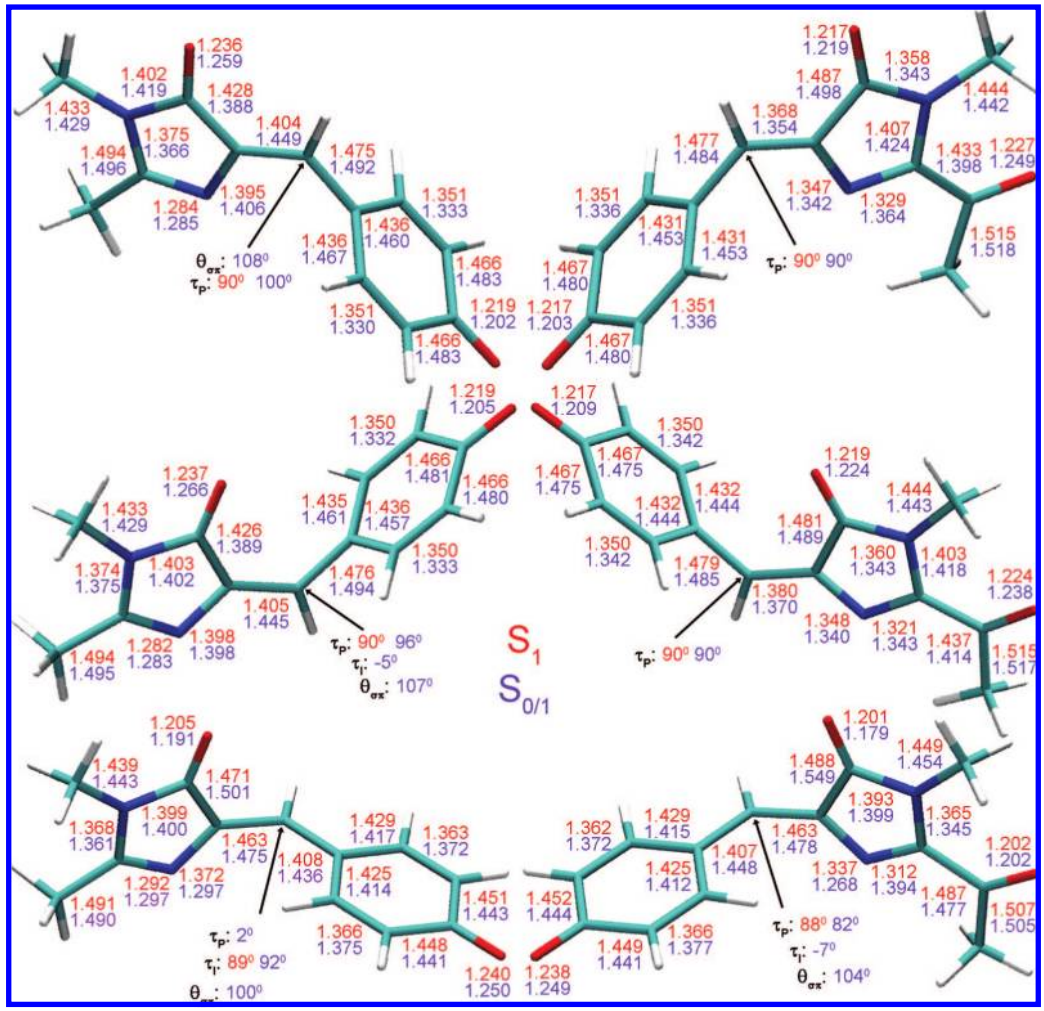

Figure 9. Geometrical details (heavy atom bond lengths in Å, selected torsion (τ_I, τ_P), and pyramidalization (θ_π) coordinates in degrees) of the *Z*-P-S_1 and *Z*-P-$S_{0/1}$ (top) twisted structures of HBDI (left) and AHBMI (right), the *E*-P-S_1 and *E*-P-$S_{0/1}$ structures (middle), and the I-S_1 and I-$S_{0/1}$ structures (bottom). Red lettering indicates S_1 intermediates, while purple lettering indicates minimal energy conical intersections (MECIs). Bonds (atoms) for which torsion (pyramidalization) coordinates are listed are indicated by arrows. Torsions within 1° of 0° and 180° are not shown, as are pyramidalization angles within 1° of 90°. All structures were generated at the SA3-CAS(4,3)/DZP level.

E HBDI are displayed in Figure 10. Similar slices for *Z* and *E* AHBMI are displayed in Figure 11. Table 2 collects the highest sampled S_1 energy along all coordinate driving pathways and compares this to the energy at the appropriate Plan-S_1 geometries. The highest sampled energies are beneath the Franck−Condon (Min-S_0) S_1 energy with one exception, along the path from *Z*-Min-S_0 to I-S_1 in AHBMI. The highest sampled energy along this pathway is 3 kcal/mol above the S_1 energy at *Z*-Min-S_0, suggesting that the pathway is closed. This result should be confirmed later via a more rigorous transition state search. Comparing to the Plan-S_1 energies (coinciding with the energies in Figures 10 and 11 with zero twist), our results suggest, but do not prove, the presence of barriers to isomerization on the excited-state in all cases except for the path leading from *E*-Plan-S_1 to I-S_1 in HBDI, which is straight downhill on S_1. In the limit of sufficient sampling, the coordinate-driven pathway indicates an upper bound to the true activation energy. Therefore, our results indicate barrierless imidazolinone photoisomerization in *E*-HBDI. They suggest, but do not prove, a small barrier to photoisomerization in *Z*-HBDI and *E*-AHBMI and more substantial barriers to photoisomerization in *Z*-AHBMI. These latter results should be confirmed via transition state search.

Gas phase studies of HBDI anion[55] estimate the excited-state lifetime to be ~100 μs, which is considerably longer than the <5 ps ground-state recovery time in alcohol solutions.[11] The lifetime in gas phase was estimated via the decay of neutral species produced by a two-photon photoionization process. The long decay time of HBDI in vacuum suggests that a barrier to photoisomerization may exist though no temperature-dependent study was undertaken. The small upper boundary to photoisomerization barriers which we have calculated for *Z*-HBDI are consistent with this if we postulate a reduced frequency of twisting attempts due to a flatter potential surface in the excited state. *Z*-HBDI is known to be the dominant isomer in alkaline solutions[39] such as were used to generate the gas-phase ions via an electrospray mechanism.[55]

Discussion

We have reported side-by-side studies of the S_0 and S_1 electronic structure and potential energy surfaces of HBDI and AHBMI anions, two synthetic model chromophores representing the GFP and KFP subfamilies of the fluorescent proteins. These compounds differ only in the substituent at the 2-position of the imidazolinone, being either methyl (GFP) or acetyl (AHBMI), but they display qualitative differences in the photoi-

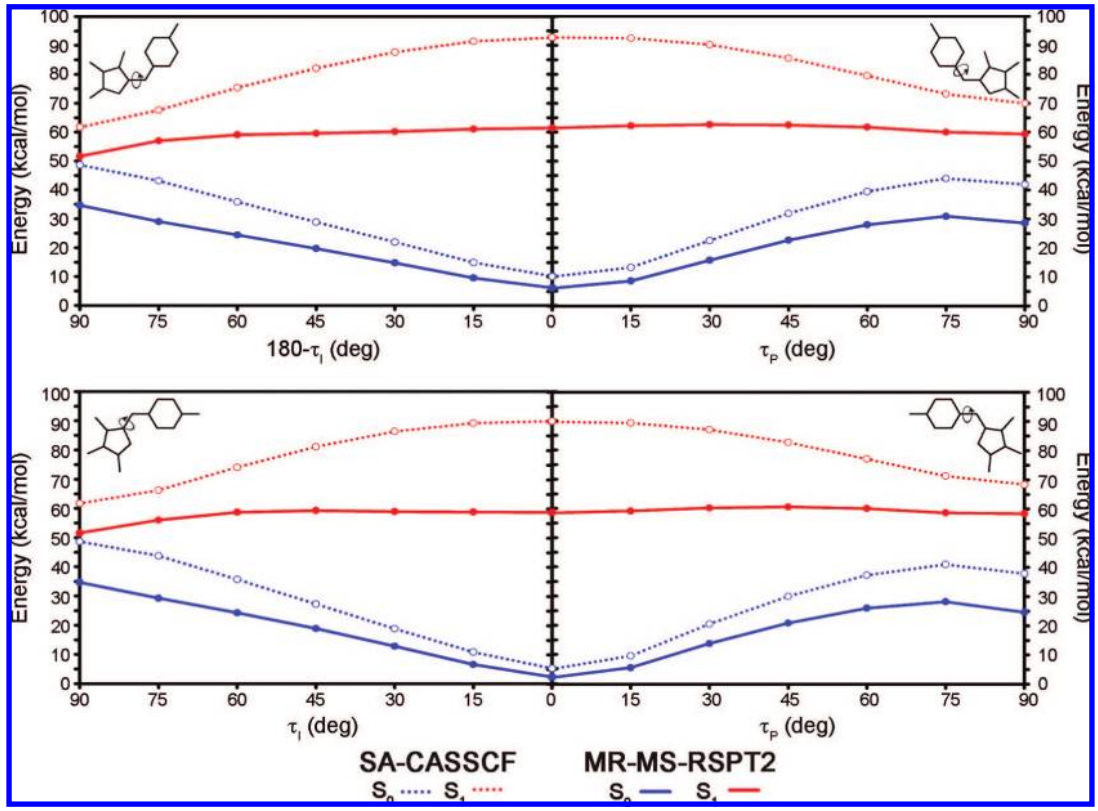

Figure 10. Imidazolinone bond torsion (τ_I, left) and phenoxy bond torsion (τ_P, right) coordinate-driven potential surface slices for *E*(top) and *Z*(bottom) HBDI at the SA3-CAS(4,3)/DZP (dotted lines) and MR-MS-RSPT2 (solid lines) levels. Coordinate-driven pathways were generated by constraint of one torsional coordinate to a fixed value, the other to zero, and optimization of all remaining coordinates on the SA3-CAS(4,3)/DZP S_1 surface. Solid and open circles indicate sampling points.

somerization energetics. Several of our results suggest different bond selection regimes for HBDI and AHBMI: the relative energies of TICT intermediates and MECIs, the bond alternation at planar geometries, and S_1 energies sampled along coordinate-driving slices through the potential surface. They suggest selection for imidazolinone bond photoisomerization in HBDI anion and phenoxy bond photoisomerization in AHBMI. They also suggest that bond selection depends on whether the reaction proceeds from a *Z* or an *E* initial configuration.

Resonant Lewis structures can be drawn for anionic HBI derivatives which differ by the position of the π bond on the bridge and by the location of a formal negative charge, which can be localized on either the phenoxy or the imidazolinone. At planar geometries, transition to the twin excited state[17] is optically allowed. This inverts the resonance and creates a delocalized biradical structure on the bridge. Some localization of the biradical occurs following relaxation on S_1 under constraint of a planar bridge configuration. If the constraint of planarity is relaxed, the biradical completely localizes on one the other bond as it twists, and the system accesses a manifold of twisted internal charge transfer (TICT) states.[59] The specific TICT state accessed depends on the identity of the twisted bond. The TICT states can be distinguished by the polarity of the charge localization in the S_0 and S_1 states. The S_0/S_1 energy gap shrinks upon TICT state[59] formation, and bridge-twisted MECIs have been shown to occur in HBI,[20] HBDI, and AHBMI and in a truncated red FP chromophore model (4-*p*-hydroxybenzylidene-2-(*N*)-acylimine-imidazolin-5-one).[21] The MECIs can be correlated by geometric similarity to one or the other TICT intermediates, via identification of the (most) twisted bond. The intersection seams arise from the crossing of diabatic valence-bond states with opposing charge localization across the twisted bond. Diabatic states with opposing localization come to dominate the S_0 and S_1 states at twisted geometries, so that charge localization persists in the adiabatic states. In addition to the MECIs reported here, 'hula-twisted' MECIs have also been reported.[18,19] These also possess charge-transfer character, but they are not energetically accessible on the S_1 state *in vacuo*. They have not been convincingly established as important to internal conversion via bridge photoisomerization.

Comparison with Previous Results for GFP Chromophore Models. The relatively long gas-phase excited-state lifetime[55] of HBDI anion suggests the existence of barriers to photoisomerization. On the other hand, HBDI anion displays ultrafast decay in aqueous[10] and alcohol[6–8] solutions. This was behind early suggestions for the existence of a bridge photoisomerization reaction.[60] The decay of anionic HBDI in water is longer than that of neutral and cationic forms.[10] This is interesting because, in contrast to the anion, neutral and cationic HBDI are predicted by ab initio calculations[20] to favor only a single photoisomerization pathway. The pattern may arise from a flatter torsional potential surface for the anion, leading to ambiguous excited-state dynamics at short time scales.

It is informative to examine our results alongside previous MCSCF and RSPT2 studies[18–20] of the photoisomerization surfaces of HBDI and its demethylated analogue HBI. The photoisomerization reaction of HBDI has been studied by Altoe et al.[18] using an SA2-CAS(12,11)/6-31G* wave function with

(60) Niwa, H.; Inouye, S.; Hirano, T.; Matsuno, T.; Kojima, S.; Kubota, M.; Ohashi, M.; Tsuji, F. I. *Proc. Natl. Acad. Sci. U.S.A.* **1996**, *93*, 13617–13622.

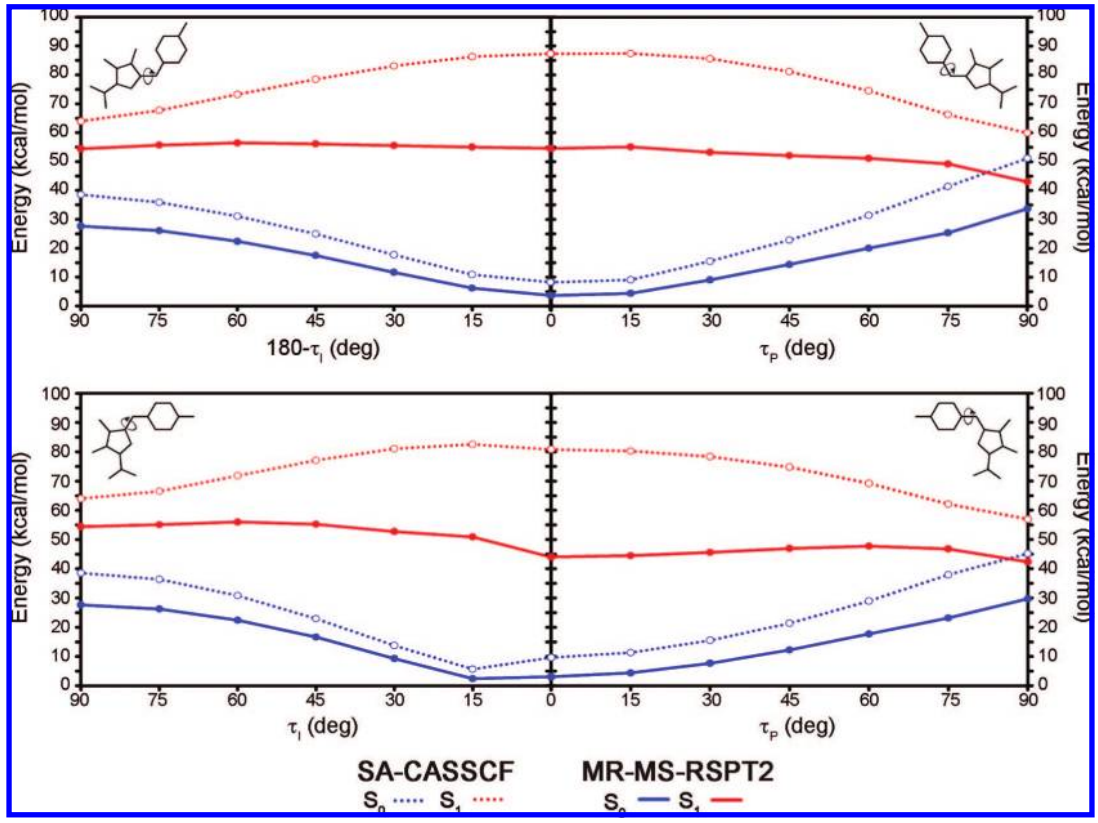

Figure 11. Imidazolinone torsion (τ_I, left) and phenoxy torsion (τ_P, right) coordinate-driven potential surface slices for *E*(top) and *Z*(bottom) AHBMI at the SA3-CAS(4,3)/DZP (dotted lines) and MR-MS-RSPT2 (solid lines) levels.. Coordinate-driven pathways were generated by constraint of one torsional coordinate to a fixed value, the other to zero, and optimization of all remaining coordinates on the SA3-CAS(4,3)/DZP S_1 surface. Solid and open circles indicate sampling points.

Table 2. Highest Sampled MR-MS-RSPT2 S_1 Energies along SA3-CAS(4,3)/DZP (τ_P,τ_I) Coordinate-Driven Potential Surface Slices[a]

start	end	Highest Sampled S_1 energy (kcal/mol)
HBDI		
E-Plan-S_1	*E*-P-S_1	2
	I-S_1	0
Z-Plan-S_1	*Z*-P-S_1	2
	I-S_1	1
AHBMI		
E-Plan-S_1	*E*-P-S_1	1
	I-S_1	2
Z-Plan-S_1	*Z*-P-S_1	4
	I-S_1	12 (3)

[a] Energies are rounded to highest whole kcal/mol and are referenced to the energy of the starting structure (left column). Values in parentheses are referenced to the S_1 energy at the Min-S_0 structure for that isomer.

single-state perturbation theory *in vacuo* and in a polarizable environment. There are qualitative differences between our results and those obtained by Altoe et al.[18] for HBDI *in vacuo*. Altoe et al. found S_1 intermediates analogous to those we report but with different energetic ordering. They describe a phenoxy twisted intermediate (corresponding to *Z*-P-S_1) which lies 6 kcal/mol lower than a relaxed S_1 planar structure (corresponding to *Z*-Plan-S_1) *in vacuo*, as well an imidazolinone-twisted intermediate (I-S_1) which lies 2 kcal/mol *above* the planar structure and is isoenergetic with the Franck−Condon region. This is in qualitative contradiction to our results, which predict a lower energy for I-S_1 than for *Z* and *E*-P-S_1. Upon immersion of the model in a polarizable continuum, Altoe et al.[18] found the energy of the I-S_1 analogue was lowered and the energetic ordering of the twisted intermediates reversed, the I-S_1 analogue now lying beneath the *Z*-P-S_1 analogue by 8 kcal/mol. The polarizable environment also changed the bridge bond alternation of the planar Min-S_0 and *Z*-Plan-S_1 analogues, with the phenoxy bond shortest *in vacuo* and the imidazolinone bond shortest in the polarizable environment. Along with these changes, the authors report a blue shift of the S_0-S_1 splitting. This mirrors a similar shift which is experimentally known to occur in aqueous solutions of HBDI anion. However, this blue shift has since been shown to arise from solvent proticity rather than polarization effects.[61]

A comparison of the results of Altoe et al.[18] with previous results reported by Martin et al.[18] for HBI *in vacuo* is a an appropriate way to examine the effect of methylation of the imidazolinone on the photoisomerization pathways. Both groups used an identical SA2-CAS(12,11)6-31G* with single-state RSPT2 methodology. They also describe identical choices of orbitals to span the active space. Both groups reported twisted intermediates for a *Z* isomer of HBDI (HBI) analogous to our *Z*-P-S_1 and I-S_1 intermediates. In the HBI case, Martin et al.[18] reported that the twisted intermediates are nearly degenerate on S_1, with the I-S_1 analogue lower in energy by only 2 kcal/mol. This is a reversal of the ordering of the HBDI twisted intermediates reported by Altoe et al.[18] Altoe et al.'s[18] and Martin et al.'s[19] predictions for the energy of the I-S_1 intermediates of HBDI and HBI, respectively, are at odds with trends

(61) Dong, J.; Solntsev, K. M.; Tolbert, L. M. *J. Am. Chem. Soc.* **2006**, *128*, 12038–12039.

which we have observed here and in previous comparisons.[21] These trends suggest that the I-S_1 intermediate should be *stabilized* by electron-donating substituents to the imidazolinone and *raised* by electron-withdrawing substituents. This is counter to the results of Altoe et al.,[18] who calculated the I-S_1 analogue of HBDI to be *destabilized* in comparison to the HBI results reported by Martin et al.[19] with apparently identical methodology.

Neither Altoe et al.[18] nor Martin et al.[19] report minimal energy conical intersections (MECIs) corresponding to those reported for HBDI here. They do report a 'hula-twist' intersection, which is twisted about both bonds in opposite phase. This intersection was invoked by Martin et al. to present a complete decay mechanism for *Z*-HBI, though it was predicted to be energetically inaccessible *in vacuo*. During the preliminary stages of this work we examined a coordinate-driving model of a hula-twist pathway. We found as well that it leads to S_0/S_1 degeneracy at the SA-CASSCF level and that it lies above the Franck−Condon energy at the MR-MS-RSPT2 level. This intersection point is not likely to participate directly in gas-phase decay processes. Its energetics in a polarizable environment[18] suggest that it may not play a role in polar solutions, either. It remains to be seen whether this segment of S_0/S_1 conical intersection seam is relevant to the protein photophysics. Most reported analyses[31,62] of hula-twist motion in the protein were based on classical molecular mechanics models that cannot describe the changes in charge localization associated with the TICT manifold.

The upper bounds to photoisomerization barriers which we report were obtained by sampling along a coordinate-driven pathway. They provide an upper bound to the activation energy in the limit of sufficient sampling. Martin et al.[19] reported photoisomerization barriers for *Z*-HBI obtained by sampling along a minimum energy path determined by minimization on successive hyperspherical surfaces in mass weighted coordinate space. The barrier quoted for passage to the I-S_1 analogue from the *Z*-Plan-S_1 analogue was 1 kcal/mol, in agreement with our upper bound for HBDI using a coordinate-driving pathway. Altoe et al.[18] did not quote barrier heights for photoisomerization of *Z*-HBDI, but they do remark that it is within the 1−2 kcal/mol ambiguity threshold for RSPT2 energetics. This also agrees with our current results.

Semiempirical analyses of structures and energetics relevant to photoisomerization in HBI anion have been reported by Voityuk et al.[63] using AM1/CISD, by Weber et al.[58] using OM2/PertCI, and by Toniolo et al.[22,23] using a floating occupation molecular orbital (FOMO) semiempirical CAS-CI model reparametrized against *ab initio* results. The observations made by Voityuk et al.[63] and of Weber et al.[58] are qualitatively similar to our own, predicting favorable excited-state twisting about either exocyclic bond in *Z*-HBDI anion but no favorable hula-twist. No MECIs were reported in either case. The FOMO CAS-CI method of Toniolo et al.[22,23] is capable of optimizing MECIs,[64] but in this case the *ab initio* MECIs were used as input to the parametrization so no prediction was made. The *ab initio* MECIs used in the parametrization were analogous to those reported here and generated with an HBI model. The model was subsequently used in QM/MM multiple spawning simulations[23] which indicated ultrafast excited-state decay in a cluster of water molecules. It was also used to calculate a minimum energy path in the protein environment,[65] which indicated a barrier to photoisomerization in the protein. Both results are broadly consistent with experimental observations of ultrafast decay of HBI in solution[10] and of high fluorescence quantum yield in GFP from *A. victoria*.[1]

Comparison with Previous Results for KFP Chromophore Models. Knowledge of the KFP subfamily of the fluorescent proteins is considerably newer than the GFP subfamily, so there is less data with which to compare. The first member of the subfamily (asFP595)[34] was reported in 2000 and controversies surrounding the chromophore chemistry have only been recently resolved.[36] To the best of our knowledge, there is only one experimental report of AHBMI, which accompanied the report of its synthesis.[41] The gas-phase absorption of AHBMI has not been reported. The absorption of the AHBMI anion in solution is red-shifted relative to HBDI and depends on both polarity and proticity of the solvent.[61] Interestingly, the compound displays weak fluorescence in DMF solution[41] with the fluorescence quantum yield an order of magnitude higher than that of the native (dark) state of asFP595[33] and with a similar emission wavelength.[34] No significant fluorescence was reported in protic solvents, regardless of bulk dielectric. HBDI anion also displays a red shift in DMF compared to protic solvents but without detectable fluorescence.[61]

Our results for AHBMI *in vacuo* suggest that the imidazolinone-bond photoisomerization pathway may be more effectively suppressed than either pathway in HBDI. We postulate based on the electronic structure of the TICT states that this arises due the greater electron affinity of the acetyl substituent relative to methyl. This stabilizes charge accumulation on the imidazole, in accord with the character of the P-S_1 intermediates but opposite to the character of the I-S_1 intermediates. We have invoked a similar effect to rationalize the photoisomerization surfaces of 4-*p*-hydroxybenzylidene-2-(*N*)-acylimine-imidazolinone, a model of the chromophore of the RFP subfamily.[21] This chromophore is an intermediate in the maturation of KFP chromophore.[66] Here, we always use 'KFP chromophore model' to refer only to models of mature (acetyl-substituted) KFP chromophores.

Progress from the planar intermediates toward twisted intermediates in HBDI and in AHBMI is accompanied by large changes in the electronic state dipoles. The changes upon twisting different bonds are not identical. Specifically, the S_1 dipole is much larger than the S_0 dipole at the I-S_1 intermediate whereas the opposite is true at the P-S_1intermediates. This is because the 'positive end' of the dipole points toward localized positive charge on the imidazolinone in either case, whereas the negative end will point toward either the imidazolinone oxygen (in the S_0 state at I-S_1 or the S_1 state at *Z*,*E*-P-S_1) or toward the phenoxy (S_1 state at I-S_1 or S_0 state at *Z*,*E*-P-S_1) depending on which bond twists. We observe this behavior for both HBDI and AHBMI models. In AHBMI the dipole norm is somewhat smaller, which may be due to conjugation with the nearby acetyl. We postulate that AHBMI in DMF exists in a regime where the polar solvent does not stabilize the I-S_1

(62) Baffour-Awuah, N. Y. A.; Zimmer, M. *Chem. Phys.* **2004**, *303*, 7–11.
(63) Voityuk, A. A.; Michel-Beyerle, M.; Rösch, N. *Chem. Phys. Lett.* **1998**, *296*, 269–276.
(64) Toniolo, A.; Ben-Nun, M.; Martinez, T. J. *J. Phys. Chem.* **2002**, *A106* (18), 4679–4689.
(65) Olsen, S.; Toniolo, A.; Ko, C.; Manohar, L.; Lamothe, K.; Martinez, T. J. Computation of Reaction Mechanisms and Dynamics in Photobiology. In *Computational Photochemistry*; Olivucci, M. Ed.; Elsevier: Amsterdam, 2005.
(66) Martynov, V. I.; Savitsky, A. P.; Martynova, N. Y.; Savitsky, P. A.; Lukyanov, K. A.; Lukyanov, S. A. *J. Biol. Chem.* **2001**, *276* (24), 21012–21016.

intermediate such that this pathway becomes barrierless but *does* destabilize the P-S_1 intermediates relative to the S_1 planar configurations (possibly in tandem with changes to the planar configurations themselves). This may explain the weak fluorescence observed for AHBMI anion in DMF solution. Continuing this line of thought, solvation in nonprotic solvents with increasing dielectric constant may further stabilize the I-S_1 intermediate to a point where the photoisomerization pathway can be accessed, leading to loss of fluorescence. Future observation of a regime where increasing the dielectric constant (in a nonprotic solvent) reduces the fluorescence quantum yield may therefore be taken as support of this hypothesis. The reader may recognize that this argument implicitly postulates a linear free energy (Hammett)[67,68] relationship for photoisomerization about the imidazolinone bond. A similar relationship has recently been demonstrated[69] for the photoisomerization of hemithioindigo compounds, which possess a similar methine bridge chemistry.

Implications for Photophysics of GFPs and KFPs. There are now several high-resolution crystal structures available which indicate that fluorescent and nonfluorescent populations of FPs are distinguished by *Z*/*E*-isomerism of the imidazolinone bond.[29–32,35,37,38,70,71] Particularly interesting cases are those where switching between fluorescent and nonfluorescent states can be achieved with specific illumination regimes.[29,33,34,72] Not all nonfluorescent proteins display photoswitching behavior,[71] and not all FPs with a chromophore in an *E*-configuration are nonfluorescent.[73] Nonfluorescent FPs with an *E* chromophore tend to display twist about the phenoxy bond[71] in their ground-state structures. Nonplanarity of the phenoxy bond in the ground state suggests decay by phenoxy photoisomerization even more than by imidazolinone photoisomerization, as it will lead to increased phenoxy photoisomerization attempts at shorter timescales in the excited state. However, phenoxy bond isomerism cannot serve as a switch between distinguishable populations because isomerization maps the initial conformation to itself. Given the currently available picture of FP chromophore electronic structure, it seems natural to postulate that selection between photoswitching and ground-state recovery may correspond, at the molecular level, to selection between photoisomerization of distinct bonds of the bridge. Within this context, photoisomerization of the phenoxy bond is to be associated with ground-state recovery, while photoisomerization of the imidazolinone bond is to be associated with either photoswitching (by decay leading to successful isomerization) or ground-state recovery (by decay leading to unsuccessful isomerization).

Imidazolinone bond and phenoxy bond photoisomerization appear, on the basis of present and previous[18–22,58] results, to be associated with disjoint basins on the S_1 potential surface and with distinguishable and opposing charge localizations between the rings and the bridge. It seems, *prima facie*, that even if all the relevant intersections are topologically indistinct, the specific regions which are accessed may be distinguished by the charge localization as they are approached. If imidazolinone and phenoxy photoisomerization can be associated with distinct families of dynamical paths, then classical interactions with the environment may be adequate to select between different reaction outcomes. Such interactions may be described by QM/MM simulations.[74] If the photoisomerization dynamics leading to different reaction outcomes are not distinguishable, then some quantum character of the chromophore−environment interaction may be invoked in order to explain selection by the protein of one pathway over another.

Forward and reverse photoswitching is accomplished by similar mechanisms in both KFPs and GFPs, but the nature of the dark-adapted and photoswitched states are reversed between the two. Forward switching (from the dark-adapted state) is accomplished by high intensity light at the absorption maximum. It renders GFPs like Dronpa and mTFP0.7 nonfluorescent and renders KFPs asFP595 and KFP1 fluorescent. Reverse photoswitching occurs under moderate intensity light at higher energies.[29,33,34,72] Fluorescent and nonfluorescent states are identified with *Z* and *E* chromophores, respectively, so dark-adapted photoswitching GFPs carry a *Z* chromophore[35,75] while dark-adapted KFPs carry *E*.[31,32] It is clear that bridge photoisomerization is not the only chemistry involved in the switching. Evidence suggests that chromophores of photoswitching GFPs such as Dronpa[76] and mTFP0.7[29] become protonated in their nonfluorescent state. A time-resolved fluorescence study of Dronpa concluded that excited-state deprotonation is likely to be the first step in the backward photoswitching reaction,[77] so that subsequent *Z*/*E* photoisomerization would occur as an anion. For photoswitching KFPs, there is less direct evidence implicating a neutral chromophore in the nonfluorescent state, although it has been suggested.[78] We noted with interest that the S_0-S_2 energy gap of *Z*-AHBMI predicted by our model (2.64 eV) was very close to the excitation energy required for reverse switching in asFP595 (2.76 eV), and that the electronic structure suggested a possibility for altered selectivity in the dynamics following excitation to this state. However, the oscillator strength was very low, arguing against its assignment to the high-energy excitation that initiates backward switching in asFP595 and KFP1. The apparent tendency of AHBMI to favor phenoxy-twist in the excited-state seems to mirror the nonfluorescence of the native state of asFP595, which carries an *E* chromophore with a phenoxy bond that is nonplanar in the ground state.[31,32] Likewise, the suggestion that excess energy is needed in order to carry out imidazolinone photoisomerization may underlie the excitation-dependence of the forward switching reaction in this protein.[79] Ultimately, any interesting parallels we observe between our results and protein trends must be tempered by the recognition that we have performed our calculations *in*

(67) Hammett, L. P. *Chem. Rev.* **1935**, *17* (1), 125–136.
(68) Hammett, L. P. *J. Am. Chem. Soc.* **1937**, *59* (1), 96–103.
(69) Cordes, T.; Schadendorf, T.; Priewisch, B.; Ruck-Braun, K.; Zinth, W. *J. Phys. Chem.* **2008**, *A112* (4), 581–588.
(70) Battad, J. M.; Wilmann, P. G.; Olsen, S.; Byres, E.; Smith, S. C.; Dove, S. G.; Turcic, K. N.; Devenish, R. J.; Rossjohn, J.; Prescott, M. *J. Mol. Biol.* **2007**, *368* (4), 998–1010.
(71) Prescott, M.; Ling, M.; Beddoe, T.; Oakley, A. J.; Dove, S.; Hoegh-Guldberg, O.; Devenish, R. J.; Rossjohn, J. *Structure* **2003**, *11*, 275–284.
(72) Ando, R.; Mizuno, H.; Miyawaki, A. *Science* **2004**, *306* (5700), 1370–1373.
(73) Petersen, J.; Wilmann, P. G.; Beddoe, T.; Oakley, A. J.; Devenish, R. J.; Prescott, M.; Rossjohn, J. *J. Biol. Chem.* **2003**, *278*, 44626–44631.
(74) Warshel, A.; Levitt, M. *J. Mol. Biol.* **1976**, *103*, 227–249.
(75) Andresen, M.; Stiel, A. C.; Trowitzsch, S.; Weber, G.; Eggeling, C.; Wahl, M. C.; Hell, S. W.; Jakobs, S. *Proc. Natl. Acad. Sci. U.S.A.* **2007**, *104* (32), 13005–13009.
(76) Habuchi, S.; Ando, R.; Dedecker, P.; Verheijen, W.; Mizuno, H.; Miyawaki, A.; Hofkens, J. *Proc. Natl. Acad. Sci. U.S.A.* **2005**, *102* (27), 9511–9516.
(77) Fron, E.; Flors, C.; Schweitzer, G.; Habuchi, S.; Mizuno, H.; Ando, R.; DeSchryver, F. C.; Miyawaki, A.; Hofkens, J. *J. Am. Chem. Soc.* **2007**, *129* (16), 4870–4871.
(78) Schäfer, Lars, V.; Groenhof, G.; Klingen, Astrid, R.; Ullmann, G. M.; Boggio-Pasqua, M.; Robb, Michael, A.; Grubmüller, H. *Angew. Chem., Int. Ed.* **2007**, *46* (4), 530–536.

vacuo. Conclusive statements about the protein photoreaction would require some consideration of the environment.

Conclusions

We have characterized the S_1 surfaces of model chromophores from two FP subfamilies where photoswitching is associated with $Z-E$ isomerism of the bridge. Our results reinforce the view that charge-localized states play a central role in the bridge photoisomerization of FP chromophore anions. Among the more important results is the suggestion of different bond selection regimes in the bridge photoisomerization of GFP and KFP chromophore anions. We postulate that follows from differential effects of the substituency of GFP and KFP chromophores on the TICT states that mediate the internal conversion events. Other results of interest include indications of increased tendency for imidazolinone photoisomerization following excitation of the *E* isomer. Our results, obtained *in vacuo* for these models, are intended to serve as predictions of future gas-phase results, tools for the interpretation of those currently available, or as indicators of innate chromophore chemistry to which later environment-inclusive models may be compared. Without such a reference, it would be impossible to identify where the protein enters into an appropriate selection mechanism.

Acknowledgment. We thank M. Prescott for informative discussions about fluorescent proteins and R.H. McKenzie for help with valence-bond interpretations of the CASSCF results, as well as for comments on the manuscript. We are also grateful to the staff of the APAC National Computer Facility, and particularly D. Singleton and R. Kobayashi, for their valuable help. Time on the APAC machines was generously provided via a grant from the Merit Allocation Scheme. This work has been supported in part by funding provided by the ARC/NHMRC Research Network "Fluorescence Applications in Biotechnology and Life Sciences" (FABLS, RN0460002). Some of the figures were generated with VMD; see ref 80.

Supporting Information Available: Cartesian coordinates (Å) of reported structures, SA-CASSCF and MR-MS-RSPT2 absolute energies (hartree), SA-CASSCF and MRCISD state dipole moments and transition dipole moments, pictures of state-averaged natural orbitals, corresponding state-averaged occupation numbers, and a complete reference 53. This information is available free of charge via the Internet at http://pubs.acs.org.

JA078193E

(79) Schuttrigkeit, T. A.; von Feilitzsch, T.; Kompa, C. K.; Lukyanov, K. A.; Savitsky, A. P.; Voityuk, A. A.; Michel-Beyerle, M. E. *Chem. Phys. Lett.* **2006**, *323* (2−3), 149–160.

(80) Humphrey, W.; Dalke, A.; Schulten, K. *J. Mol. Graph.* **1996**, *14*, 33−38.